

Research Article

Failure Analysis of Locally Damaged Slender Steel Bars Strengthened with CFRP Composites: Experiments, Theory, and Computational Simulations

Bin Li ^{1,2}, Hua Luo ¹, and Xianqiao Wang ³

¹School of Civil and Architectural Engineering, Hunan Institute of Science and Technology, Yueyang 414006, China

²School of Bridge and Structure Engineering, Changsha University of Science and Technology, Changsha 410076, China

³College of Engineering, University of Georgia, Athens, GA 30622, USA

Correspondence should be addressed to Bin Li; 12007030@hnist.edu.cn

Received 19 May 2020; Revised 16 September 2020; Accepted 22 September 2020; Published 20 October 2020

Academic Editor: Melina Bosco

Copyright © 2020 Bin Li et al. This is an open access article distributed under the Creative Commons Attribution License, which permits unrestricted use, distribution, and reproduction in any medium, provided the original work is properly cited.

Carbon fiber-reinforced polymer/plastic (CFRP) composites bear attractive performance in resistance to tension, fatigue, and corrosion and, thus, have been recognized as a promising candidate for repairing and strengthening steel structures in engineering. Here, we combine experiments, theory, and numerical simulations to elucidate how the location and degree of local damages, as well as the reinforcement mode, affect the stability of slender steel bars repaired by CFRP. The deformation, failure mode, and the critical buckling load of the reinforced steel flat bars subjected to axial compressive forces are experimentally evaluated. We show that all tested specimens exhibit buckling failure, before which the damaged steel bars have entered an elastic-plastic stage. Our theoretical analysis provides an upper bound for the critical force, which is sensitive not only to the damage degree but also to the damage location. Damage locating at the middle regime of the specimens will remarkably reduce stability of the steel bars, but an optimized combination of wrapping method and number of CFRP layers can restore and even enhance the stability of the damaged structures beyond the undamaged counterparts. Finite element simulations are implemented in the same scenario as experiments, showing good agreement with our measurements. Our findings suggest that, to improve the stability of the damaged steel bars reinforced by CFRP, the load carrying capacity of the the bars, the number of CFRP layers, and the construction convenience should be taken into account.

1. Introduction

Carbon fiber-reinforced polymer/plastic (CFRP) composites have attracted much attention from research and engineering communities due to their unique advantages including noncorrosive characteristics, excellent resistance to fatigue, high stiffness and strength-to-weight ratios, ease and rapidity of erection, and reduced long-term maintenance expenses [1]. With these predominant features, CFRP composites have been increasingly employed to strengthen and repair steel structures [2–4]. Furthermore, CFRP composites can be adhesively bonded to steel structures, instead of being mechanically connected to the latter through bolt holes or welds, which may significantly engender stress concentration. These advantages can put the

unique material properties of each component of steel-CFRP systems into full play and, thereby, make the use of CFRP an attractive candidate for rehabilitating and retrofitting steel structures [3, 5]. For example, it was reported that, repaired with the particular CFRP plates, the elastic flexural stiffness of damaged beams can be restored up to 50% and the strength of damaged beams can be fully restored to their original, undamaged state [6].

Recently, CFRP composites have been leveraged to enhance the stability of steel structures such as bars, columns, beams, plates, and tubes [2, 3, 7, 8]. For instance, it has been shown that the effect of CFRP on the critical load around the weak shaft is remarkable and is more significant than that of the steel plate with the same thickness [9]. Shaat and Fam [2] performed an experiment to examine the

buckling behavior of slender hollow structural section square columns strengthened using CFRP plates with high elastic moduli. They showed that the effectiveness of the CFRP system in increasing the axial strength of the columns can be substantially enhanced by increasing the slenderness ratios. Ding [10] carried out a full-scale axial compression test on round and square steel tube specimens reinforced by CFRP, respectively. Ding's results demonstrated that the ultimate bearing capacity of specimens depended on the direction of CFRP sticking fibers. These studies showed that the high stiffness of CFRP composites is utilized to provide bracing that resists the buckling and postbuckling of steel structures subjected to axial compression [11].

Most previous studies focused on the stability of undamaged steel structures reinforced CFRP composites. However, it has been recognized that the instabilities of structures are sensitive to imperfections, especially when the structures are thin [12–14]. Both the critical loads and buckling mode can be modulated by structures' imperfections such as local damage [15, 16], mechanical heterogeneities [17, 18], and geometrical nonuniformity [19, 20]. For steel structures, local damage usually emerges due to environmental cues and unanticipated human factors; this is also one of the main demands on CFRP composites to reinforce these damaged structures. Therefore, it is of significance to examine how local damage affects the stability of steel structures strengthened by CFRP. There are a limited number of studies related to the buckling of steel-CFRP structures available in the literature. Recently, the elastic buckling behaviors of locally damaged steel tubes and bars with fiber reinforced polymer reinforcement have been theoretically investigated under axial forces [21, 22]. Nevertheless, it remains elusive how the damage degree and position, as well as reinforcement method, jointly influence the buckling and postbuckling behaviors of steel-CFRP structures.

In this paper, we use a combination of experiments and numerical simulations to address the instability of damaged slender steel bars repaired by CFRP. The failure form, deformation geometry, critical load, and postbuckling state of the steel-CFRP structure are studied. We show that the position and degree of local damage, the CFRP reinforcement method, and the CFRP paste thickness can profoundly affect the critical load and postbuckling configuration. Our experimental results are consistent with finite element simulations implemented by commercial software Abaqus.

2. Experiments

2.1. Design of Damaged Steel Columns. Q235 rectangular section steel bars were selected for test. Before the reinforcement by using CFRP, two opposite sides of the steel bars were grinded to produce imperfections, through which we mimic the local damage of steel structures induced by corrosion and so on. In the present study, we used a grinding machine that has wheel metal grinding plates with grain fineness 240# to locally grind the steel bars. Three kinds of grinding depth (t_d) were produced: $t_d = 0.5, 0.6$, and 0.7 mm, which is much smaller than the bar thickness of 12 mm, as

shown in Tables 1–3. A total of 24 steel bars were prepared. We divided the 24 steel bars according to the slenderness ratios. In Groups 1–3, the slenderness ratio was taken as 115.47, 144.34, and 173.21, respectively. In Group 1, we considered a single damage region with the same length but different locations; in Group 2, we considered two damage regions with the same length; and, in Group 3, two damage regions with the different length were introduced in the specimens. The specimen number, damage area, and CFRP reinforcement are shown in Tables 1–3. For reinforcement method, we considered three typical cases: (i) unreinforced, (ii) reinforced in damaged area only, and (iii) reinforced in the whole bar. In addition, different paste thicknesses (up to 3 layers) were used for bonding the CFRP plates.

2.2. Material Parameters. We measured the mechanical properties of the steel bars by standard unidirectional tensile tests and the values were averaged over 3 sets of independent experiments, as shown in Table 4. The mechanical properties of CFRP are given in Table 5. ZP-500 carbon fiber impregnated adhesive (Grade A) was adopted for the binder.

2.3. Specimen Preparation. The preparation of the specimens included four steps. Firstly, a grinding machine with a particle size of 240# hundred-wheel metal polishing block was used to fine-polish the prescribed damage area of the steel bars (Figure 1(a)). The grinding precision was carefully guaranteed by a Vernier caliper during the whole polishing process. Secondly, two strain gauges, denoted by G1 and G2, were pasted symmetrically at the midpoint of each specimen (Figure 1(b)). The insulation treatment of the terminals of the two strain gauges was performed. Thirdly, the impregnated glue was coated in the reinforcement area of the specimens and, then, CFRP plates were pasted on the adhesive surface induced by glue (Figure 1(c)). In the situation where only the damaged areas were reinforced, the length of CFRP plates was set as 110% of the length of the damage zone to avoid stress concentration at the junction between the damaged and the undamaged regions. Finally, two strain gauges, denoted by B1 and B2, were vertically and symmetrically pasted on the CFRP surface of the specimens to measure the longitudinal strain of CFRP *in situ* (Figure 1(d)).

2.4. Test Method. The vertical loading device is shown in Figure 1(e). Two vertical displacement sensors and two horizontal displacement sensors were arranged symmetrically on both sides of the specimen to monitor the axial and lateral displacement, respectively. The vertical loading force, axial displacement, lateral displacement, and strains of the steel bars and CFRP were collected by Donghua DH3816 Net static strain tester. The position of the strain gauges was the same for all the specimens. We used the multistage, force-controlled loading mode to compress the specimens. The incremental force at each loading stage was set as 2%–10% of the predicted limit load and maintained about 1–3 min to collect data.

TABLE 1: Damage and reinforcement of steel specimens in Group 1.

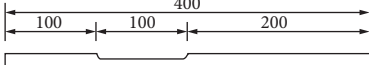
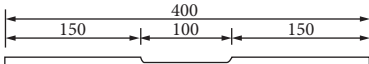
Specimen #	Geometry and damage area (cross section size 14 mm × 12 mm/ slenderness ratio 115.47)	Grinding depth t_d (mm)	Reinforcement area	Paste thickness t_n (layer)
JW000-11	Lossless steel bar	0	Unreinforced	0
JW152-12		0	Whole bar	2
JS000-13	 Unit: mm	0.5	Unreinforced	0
JS142-14		0.5	Damaged area	2
JS152-15		0.5	Whole bar	2
JS000-16		0.5	Unreinforced	0
JS142-17		0.5	Damaged area	2
JS152-18	 Unit: mm	0.5	Whole bar	2

TABLE 2: Damage and reinforcement of steel specimens in Group 2.

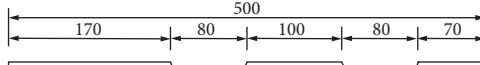
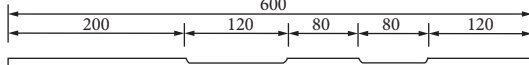
Specimen #	Geometry and damage area (cross section size 14 mm × 12 mm/ slenderness ratio 144.34)	Grinding depth t_d (mm)	Reinforcement area	Paste thickness t_n (layer)
JW000-21	Lossless steel bar	0	Unreinforced	0
JS000-22		0.5	Unreinforced	0
JS142-23	 Unit: mm	0.5	Damaged area	2
JS142-24		0.6	Damaged area	2
JS142-25		0.7	Damaged area	2
JS152-26		0.5	Whole bar	2
JS152-27		0.6	Whole bar	2
JS152-28		0.7	Whole bar	2

TABLE 3: Damage and reinforcement of steel specimens in Group 3.

Specimen #	Geometry and damage area (cross section size 16 mm × 12 mm/ slenderness ratio 173.21)	Grinding depth t_d (mm)	Reinforcement area	Paste thickness t_n (layer)
JW000-31	Lossless steel bar	0	Unreinforced	0
JS000-32		0.5	Unreinforced	0
JS141-33	 Unit: mm	0.5	Damaged area	1
JS142-34		0.5	Damaged area	2
JS143-35		0.5	Damaged area	3
JS151-36		0.5	Whole bar	1
JS152-37		0.5	Whole bar	2
JS153-38		0.5	Whole bar	3

Note. "JW" and "JS" denote undamaged and damaged specimens, respectively. From left to right, the first digits "0" and "1" represent no reinforcement and reinforcement, respectively. Second digits "4" and "5," respectively, indicate reinforcement only in damage area and reinforcement throughout full bar. The third digit represents the number of CFRP layers.

TABLE 4: Mechanical properties of steel bars.

Yield strength σ_y (MPa)	Ultimate strength σ_{bg} (MPa)	Modulus of elasticity E (GPa)
287.2	437.0	206.0

TABLE 5: Mechanical properties of CFRP.

Wide b (mm)	Density ρ (g/m ³)	Single layer thickness t_p (mm)	Tensile strength σ_{bc} (MPa)	Modulus of elasticity E (GPa)	Elongation δ (%)
200	300	0.167	3281	235.0	1.7

The specimens were strictly levelled and aligned by preloading. The preload was estimated to be 10% of the ultimate load. A slow and continuous loading method was adopted to track the whole buckling process. In our experimental tests, we added teflon spacers at the

connection between the specimens and the machine to reduce friction. In such a way, the specimens undergo weak rotation constraints at the two ends and the confinements can be approximately treated as hinged constraints.

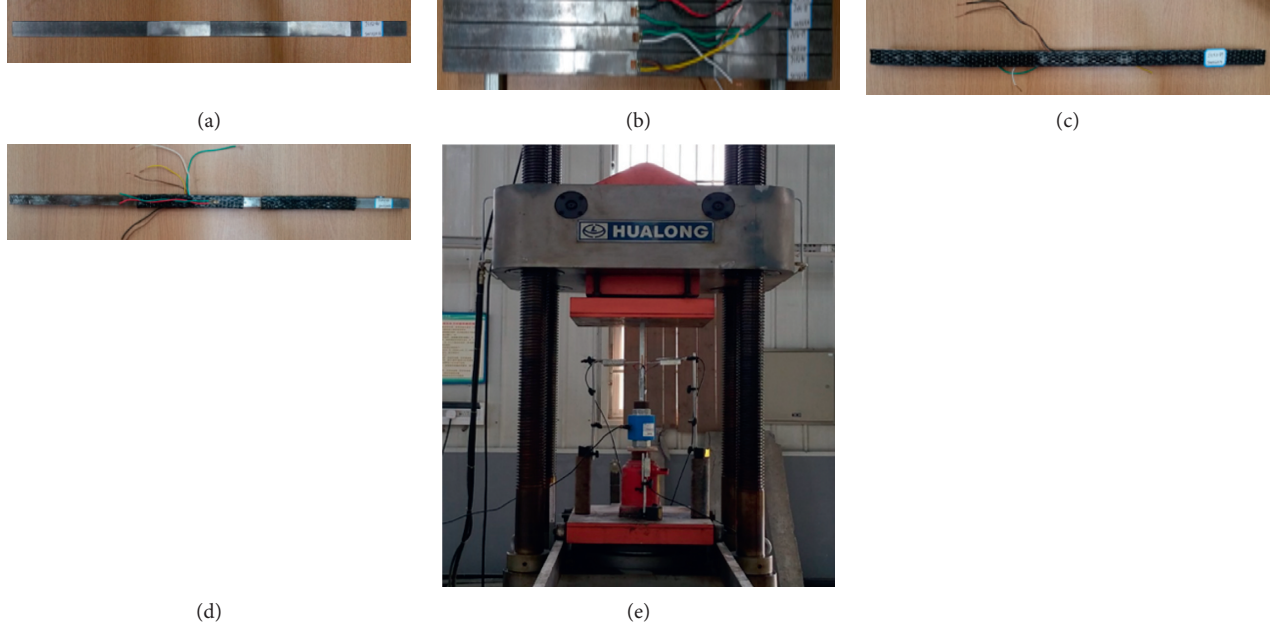


FIGURE 1: Experiment setup. (a) Grinding the damage area, (b) pasting G1 and G2 strain gauges, (c) pasting CFRP, (d) pasting B1 and B2 strain gauges, and (e) loading method.

3. Theoretical Model

We use the Bernoulli–Euler beam theory to characterize the mechanical response of both the undamaged and damaged bars. To remain consistent with experiments, we took hinged constraints at the two ends of the steel bars. The differential equation for bending of bars can be expressed as [23]

$$E_i I_i \frac{d^2 w_i}{dx^2} + F w_i = 0, \quad (1)$$

where x is the distance along the bar from the left end and subscript i denotes the region with or without damage; w_i is deflection in each region, E_i denotes Young's modulus, and I_i is the moment of inertia in different areas. F represents the axial force applied at the end. For reinforced regions, E_i stands for the effective modulus accounting for both steel bars and CFRP. For the present theoretical model, we need only to calculate the effective bending stiffness of the beam ($E_i I_i$). In the damaged regions reinforced by CFRP, we can use the transformed section method of composite beams, as shown in Figure 2, to evaluate the effective bending stiffness ($(E_i I_i)_{\text{comp}}$), which gives

$$(E_i I_i)_{\text{comp}} = \frac{B}{12} [E_s h^3 + 2E_c \delta^3 + 6E_c (H + \delta)^2 \delta], \quad (2)$$

where E_s and E_c denote Young's moduli of steel and CFRP, respectively; B is the width of the cross section of the steel bars; h is the height of the steel part in the damaged region; and δ is the total thickness of the CFRP.

The general solution of equation (1) is $w_i = A_i \sin k_i x + B_i \cos k_i x$, where $k_i = \sqrt{F/(E_i I_i)}$, and A_i and B_i are coefficients to be determined. By considering the boundary conditions at the two ends and the continuity

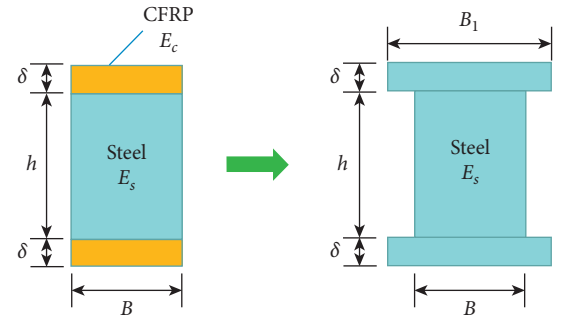


FIGURE 2: Schematic for calculating the effective stiffness of the composite section using the transformed section method, which transforms the beam into the one made of a single material of steel. B_1 denotes the width of the CFRP-reinforced zone after transformation.

conditions at the interface between damaged and undamaged regions, we can solve the critical force for buckling onset. Take Group 1 for example, where there is only one damaged region. The bar is perfect in the regions $0 < x < l_1$ and $l_2 < x < l$ and is damaged in the region $l_1 < x < l_2$, with l being the total length of the bar. Therefore, we have $w_1(0) = w_3(l) = 0$ at the two ends. The continuity conditions read $w_1(l_1) = w_2(l_1)$, $w'_1(l_1) = w'_2(l_1)$, $w_2(l_2) = w_3(l_2)$, and $w'_2(l_2) = w'_3(l_2)$. Solving this eigenvalue problem, we obtain the transcendental equation

$$\frac{k_1 \cos k_1 l_1 \sin k_2 l_0 - k_2 \sin k_1 l_1 \cos k_2 l_0}{k_2 \sin k_1 l_1 \sin k_2 l_0 - k_1 \cos k_1 l_1 \cos k_2 l_0} = \frac{k_2}{k_3} \tan k_3 (l - l_2), \quad (3)$$

where $l_0 = l_1 - l_2$. Equation (3) has to be numerically solved to calculate the critical force. For an undamaged bar

($k_1 = k_2 = k = \sqrt{F/(EI)}$), equation (3) reduces to the traditional solution $\sin kl = 0$, which gives the critical force

$$F_{cr} = \frac{\pi^2 EI}{l^2}. \quad (4)$$

The analytical method provided above is complicated when the bars have many damaged regions. In this situation, we can alternatively calculate the critical force by using energy method. We take $w = A \sin kx$ to approximate the deflection curve of the whole bar under hinged constraints at the two ends. The strain energy arising from bending (U) in the bar can be written as

$$U = \sum_{i=1,2,3,\dots} \int \frac{M^2}{2E_i I_i} dx, \quad (5)$$

where $M = Fw$. The work (T) done by the force F is

$$T = \frac{F}{2} \int_0^l \left(\frac{dw}{dx} \right)^2 dx. \quad (6)$$

The energy balance gives the critical force for buckling onset [23]. For specimens in Group 1, we obtain

$$F_{cr} = \frac{2\pi^3 E_1 E_2 I_1 I_2}{2\pi l [E_2 I_2 (l + l_0) - E_1 I_1 l_0] + l^2 (E_1 I_1 - E_2 I_2) (\sin 2\pi l_1 / l - \sin 2\pi l_2 / l)}. \quad (7)$$

This energy method can be easily extended to calculate the critical force for specimens in Groups 2 and 3.

4. Results

4.1. Buckling and Postbuckling Configuration. Our experiments showed that, at the initial stage of loading, the steel bars reduced their length and maintained a straight configuration. However, when the vertical forces were increased up to a threshold magnitude, the specimens lost stability and gave rise to buckling.

Further loading beyond the threshold increased the lateral displacement of the bars, leading to a bent, post-buckling configuration [23]. During this process, fine sound of CFRP peeling or breaking was heard in individual specimens. After the test was completed, the loading force was removed. The bent postbuckling deformation was recovered partly, while a bent configuration was still retained, as shown in Figure 3. It suggests that, under the experimental loading, the specimens entered the elastic-plastic state already.

4.2. Critical Forces and Displacements. The average of readouts of two vertical displacement sensors are taken as the axial displacement, as shown in Figure 4(a). It reveals that the axial displacement increases as axial load rises. At the initial stage of loading, the axial displacements of all specimens in each group almost coincide, indicating that the specimens bear the same axial stiffness. In other words, the effect of local damage or the reinforcement of CFRP does not emerge at this stage.

When the loading force exceeds the buckling threshold, the influence of both the local damage and CFRP appears. Take Group 1 as an example. We first compare our experimental results with theoretical prediction by equation (7) (Table 6), which shows that the experimentally measured

critical forces for all specimens are lower than the theoretical prediction. This is because of the following: (i) The energy method always gives the upper bound of the critical force. (ii) In the theoretical model, all bars are assumed to be ideal, while there exist inevitable imperfections such as defects and predeformation in experimental specimens, which reduce the real critical force.

For a damaged bar, the minimum critical force is 19.85 kN, emerging in specimen JS000-16 without reinforcement, and the maximum one is 27.99 kN, corresponding to specimen JS152-15 reinforced by CFRP covering the whole bar surface. This suggests that the CFRP can remarkably enhance the stability of the steel structures, especially when the bar is wrapped over the whole surface. Besides, it can be observed that CFRP can also enhance the critical axial displacement at the buckling onset (see specimen JW152-12). In addition, our experiment shows that the damage at the midpoint region can lower the stability of the bar more than that outside the midpoint region.

Figure 4(b) shows the relation between the loading force and the lateral displacement at the middle point of the specimens in the three groups. Before buckling onset, the lateral displacement is quite small and can be ignored. Beyond the buckling threshold, an increasing axial force induces the larger lateral displacement. Since the reinforcement of CFRP is able to enhance both the critical force and the axial displacement, a steel-CFRP structure may exhibit larger deflection during the initial postbuckling stage, compared to those unreinforced structures. This is because most of the axial displacement has been converted to the bending deformation.

4.3. Strains of Specimens. Strains of tested specimens during the whole loading process can be recorded by strain gauges. Here, we representatively show strains of Group 1 in Figure 5.

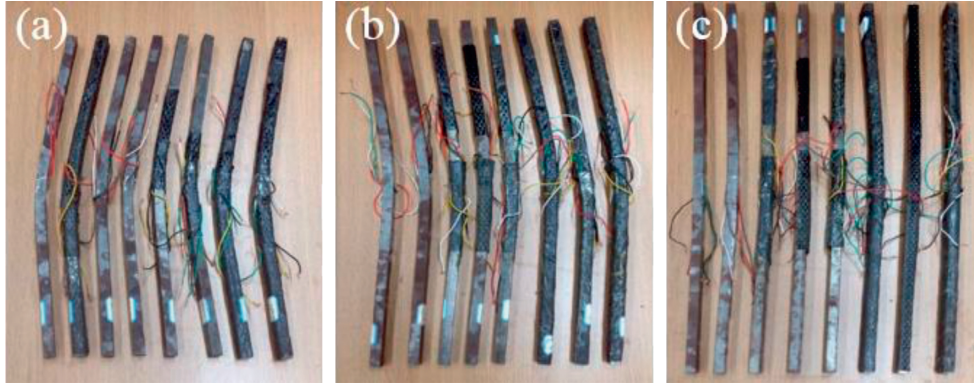


FIGURE 3: Buckling of steel bars with or without CFRP reinforcement. (a) Group 1; (b) Group 2; (c) Group 3.

Strains of Groups 2 and 3 are provided in Figures S1 and S2 in Supplementary Materials, respectively. $G1$ and $G2$ represent the longitudinal strains of the steel bars, and $B1$ and $B2$ denote the strains of the CFRP plates at the concave and the convex surface of the structure midpoint, respectively.

At the initial stage, the longitudinal compressive strains increase linearly with the increase of loading force. However, the strains on both sides are not equal, indicating that the specimens have some initial deformation or other defects. As the load continues to increase, the compressive strain $G1$ and the compressive CFRP strain $B1$ on the concave side continuously increase, while the compressive strain $G2$ and the CFRP strain $B2$ gradually transition from a compressive strain to a tensile one, suggesting that bending emerges. During this process, the longitudinal strains of the CFRP on both sides of the surface are basically consistent with the strains on the surface of the steel. It is indicated that the CFRP and the steel surface remain bonded by impregnating glue. Our experiment showed that CFRP plates are well bonded to the steel bars before axial force reaches the threshold. Beyond the threshold, strains markedly rise, while the loading forces decrease. The features of steel strains are consistent with the axial and lateral displacements shown in Figure 4. However, the CFRP strains strikingly deviate from the steel strains during postbuckling stage, which may arise from the integrated effects including the nonlinear constitutive law and surface roughness of the CFRP plates, as well as the mechanical property of the glue.

5. Factors Affecting the Critical Force

5.1. Effect of Damage Location. We first examine the influence of damage position on the buckling of the steel-CFRP structures. Our experimental data show that the critical force for specimens with damaged regions located in the center, that is, JS000-16, JS142-17, and JS152-18, is lower by 2.2%, 5.3%, and 5.9%, respectively, than that of JS000-13, JS142-14, and JS152-15 with damage outside the middle region, regardless of reinforcement method (Figure 6 and Table S1 in Supplementary Materials). It is suggested that the damage at the middle region can more significantly affect the loading

capacity of the bars than the damage at other regions. This is because a bar with end constraints in present experiment tends to undergo Euler buckling, during which the largest deflection will emerge at the middle region. Therefore, the system is quite sensitive to imperfections there.

5.2. Effect of Damage Degree. The effect of damage degree on the critical forces in Group 2 is shown in Figure 7 and Table S2 in the Supplementary Materials. In this group, different grinding thicknesses were introduced to mimic damage. Two layers of CFRP were used to reinforce the damage zones or the whole steel bars. Our experimental data show that, with local reinforcement, the critical force for damage depth $t_d = 0.5$ mm, 0.6 mm, and 0.7 mm is reduced, respectively, by 0.6%, 3.1%, and 5.3%, compared to the undamaged specimen (see specimens JS142-23, JS142-24, and JS142-25). When the whole surface of these damaged bars was wrapped with CFRP, the critical force can be enhanced by 11.3%, 7.9%, and 2.1% (see specimens JS142-26, JS142-27, and JS142-28), respectively. However, with either local or whole reinforcement, the damage depth tends to weaken the stability of the steel bars.

5.3. Effect of the CFRP Layers. The influence of the number of CFRP layers on the critical force in Group 3 is shown in Figure 8 and Table S3 in the Supplementary Materials. In this group, the steel bars are reinforced by using 1–3 layers of CFRP. It can be seen that the critical force for the damaged steel bars can be remarkably enhanced by increasing CFRP layers. When three layers of CFRP were used, the critical force for the damaged bars can be higher than that of the undamaged ones.

5.4. Effect of CFRP Reinforcement Method. In the present study, two methods, local reinforcement and whole wrapping, were employed to strengthen the damaged steel bars using CFRP. Take Group 3 as an example, as shown in Figure 8. The critical force of the specimen was completely restored and exceeded the lossless system of 7.0% when the damage zone was strengthened by using 3 layers of CFRP plate. The total length of CFRP used is 60 cm. When the whole bar was wrapped by one-layer CFRP, the critical force of the damaged specimen will completely recover and exceed the

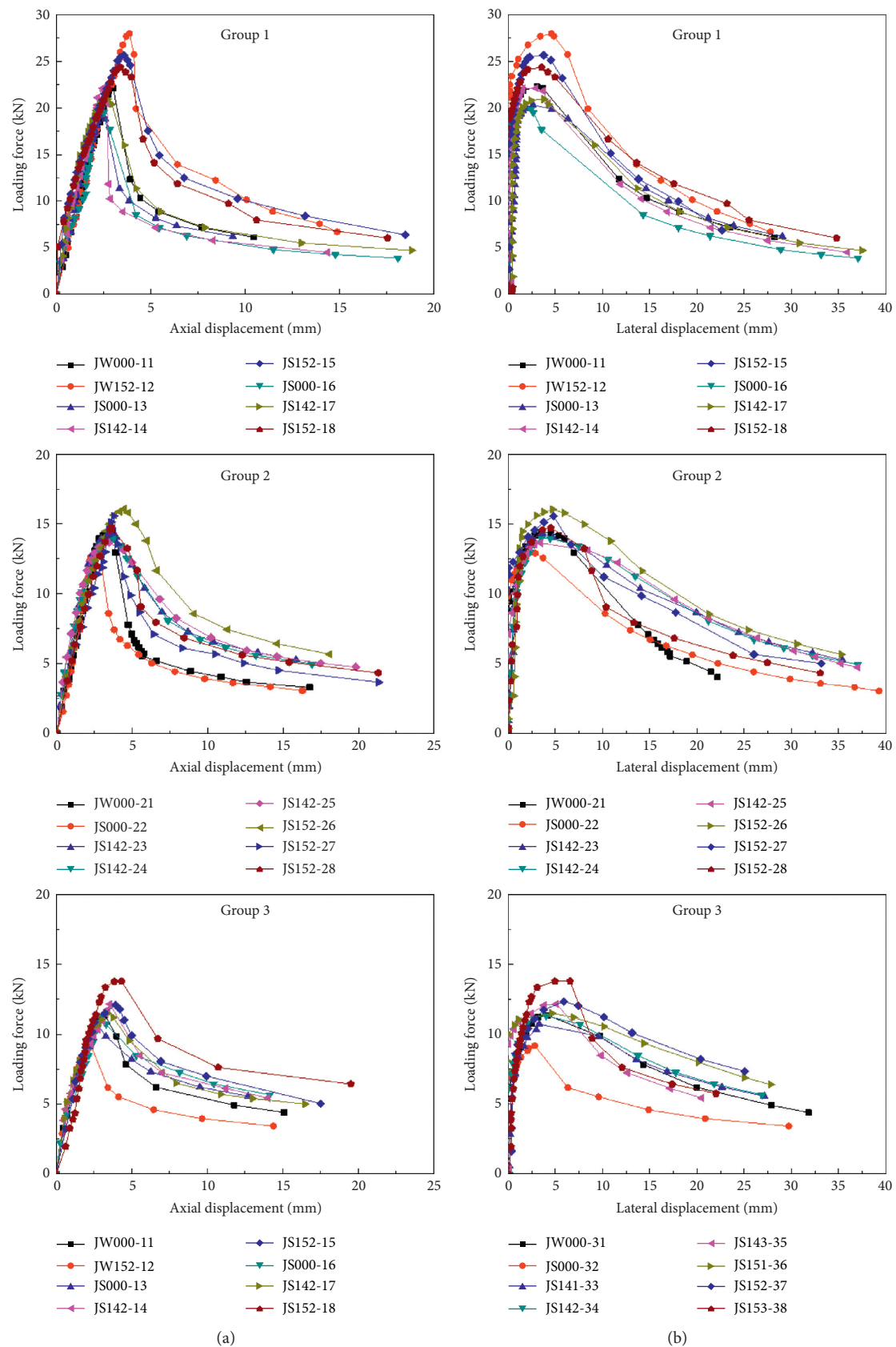


FIGURE 4: The relation between loading forces and displacements of the specimens. (a) Axial displacement; (b) lateral displacement at the midpoint.

TABLE 6: Comparison between experimental and theoretical results.

Group 1 Specimen #	Reinforcement area	Critical force F_{cr} (kN)	
		Experiment	Theory
JW000-11	Unreinforced	22.29	25.62
JW152-12	Whole bar	27.99	30.50
JS000-13	Unreinforced	20.33	22.83
JS142-14	Damaged area	22.14	24.86
JS152-15	Whole bar	25.68	27.37
JS000-16	Unreinforced	19.85	22.44
JS142-17	Damaged area	20.96	24.74
JS152-18	Whole bar	24.37	26.92

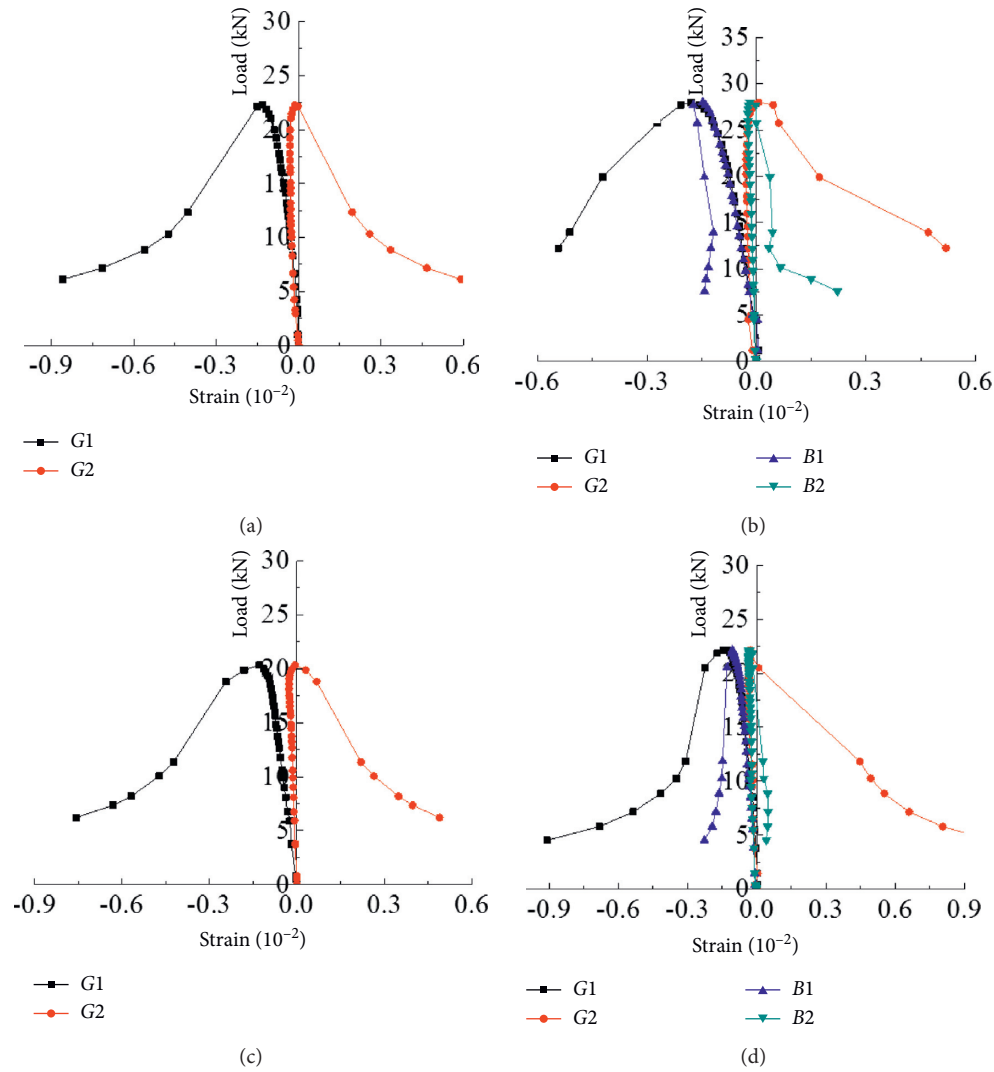


FIGURE 5: Continued.

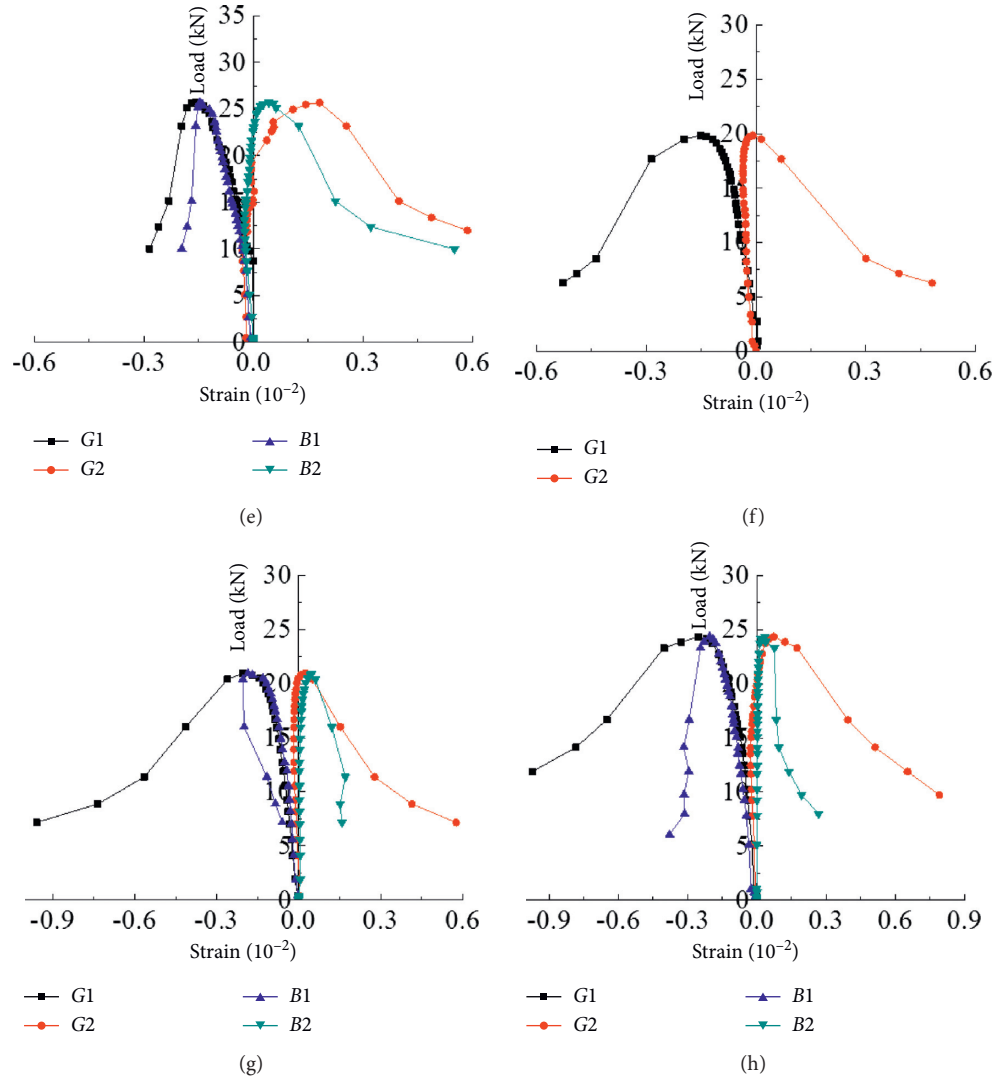


FIGURE 5: Strains of the specimens in Group 1. (a) JS000-11, (b) JW152-12, (c) JS000-13, (d) JS142-14, (e) JS152-15, (f) JS000-16, (g) JS142-17, and (h) JS152-18.

lossless component of 1.2%. In this situation, the total length of CFRP is also 60 cm. It can be seen that when the same amount of CFRP is allowed, the two reinforcement methods may give rise to similar strengthening effect on enhancing stability and recovering loading capacity of the damaged structures. Therefore, the amount of CFRP, the simplicity of the reinforcement, and the strengthening effect should be synthetically considered in engineering. As for the case in Group 3, the whole wrapping method using one layer of CFRP could be more reasonable, because it can not only simplify the construction technology but also attain the on-demand reinforcement effect.

6. Finite Element Simulation

We use the finite element method (FEM) to simulate our experiments using Abaqus software. The constitutive laws for the steel bars and CFRP are extracted from our experimental measurement, as shown in Figure 9.

Solid elements and shell elements are used to mesh the steel bars and CFRP, respectively. TIE is adopted to bond the steel and CFRP at their interface, which is basically consistent with our experimental tests. Hinged supports are prescribed at the two ends of the bars to remain consistent with our experiments. In the simulations, we reduced the cross section height according to the grinding depth in our experiments to mimic the local damage. The nonlinear buckling analysis is implemented by RIKS algorithm to consider the effects of both material and geometric nonlinearity. Simulated configurations are representatively shown in Figure 10, in consistence with experimental observation. The numerical results of the axial displacement, the lateral displacement, and the critical force are compared with experimental measurement, as shown in Figure 11 and Tables S4–S6 in the Supplementary Materials.

Although the critical force obtained by FEM simulation is slightly higher than the experimental value, the

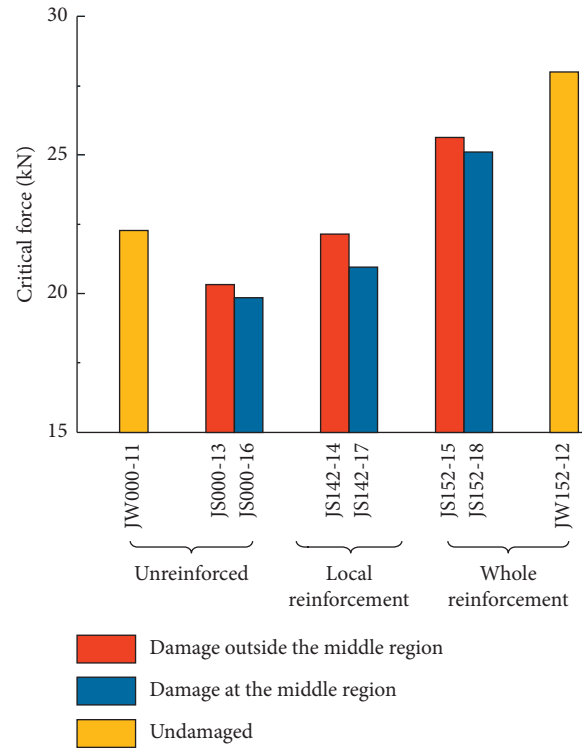


FIGURE 6: Influence of damage location on the critical force in Group 1.

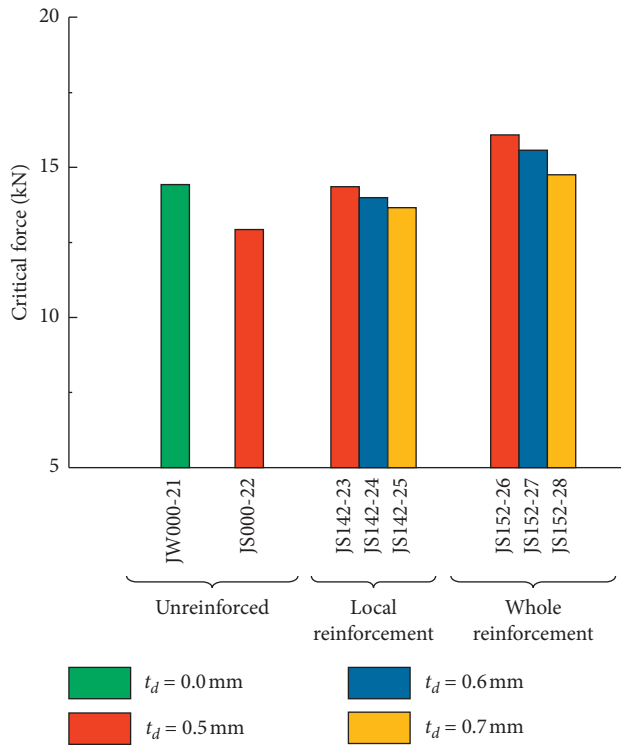


FIGURE 7: Influence of damage degree on the critical force in Group 2.

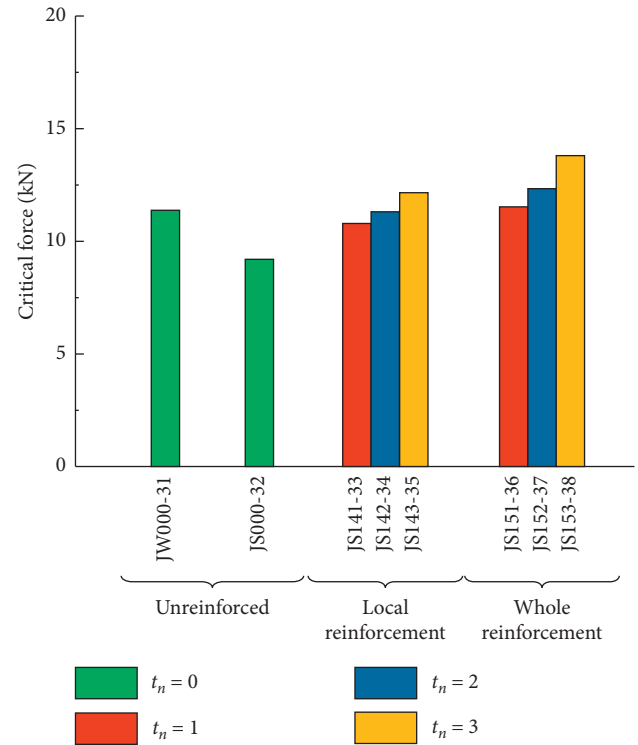


FIGURE 8: Influence of paste thickness of CFRP on the critical force in Group 3.

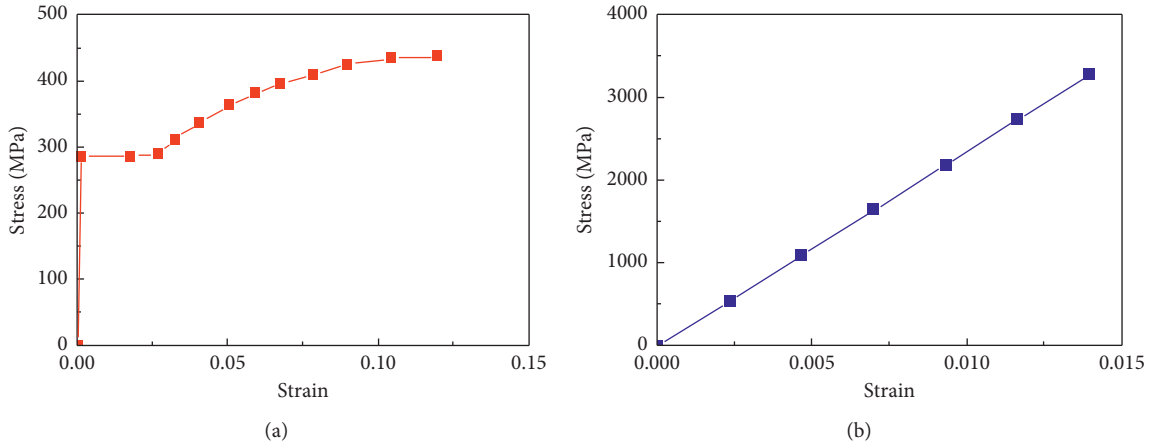


FIGURE 9: Constitutive laws. (a) Steel; (b) CFRP.

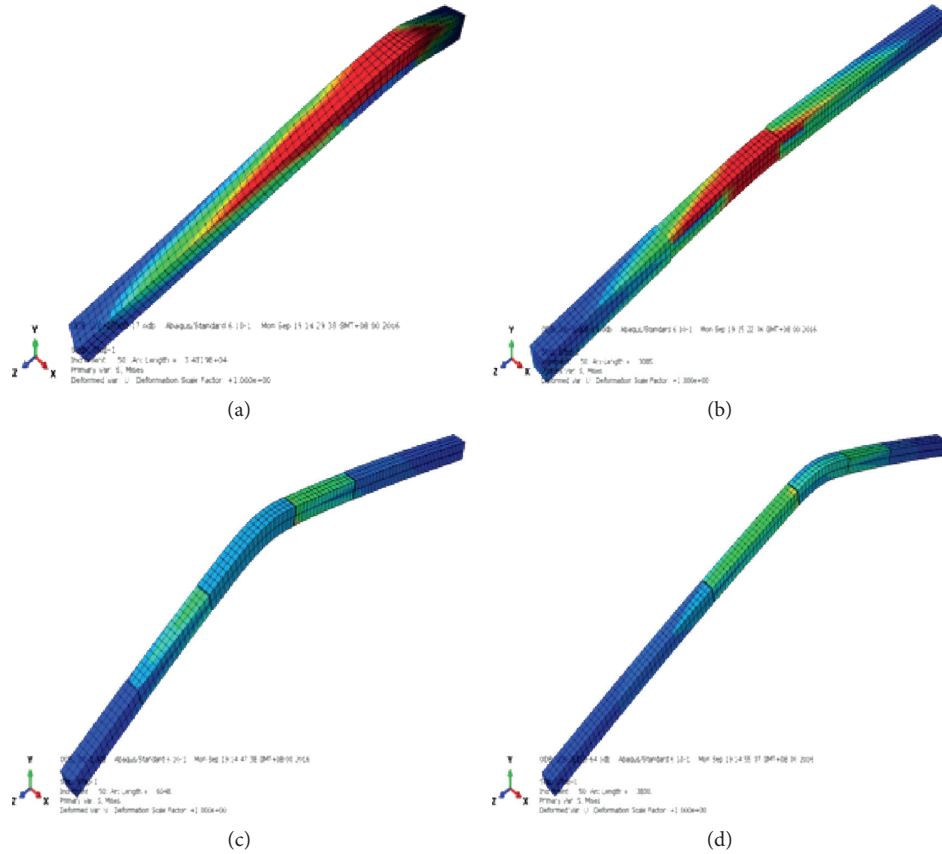


FIGURE 10: Buckling configuration of representative specimens. (a) JS000-11, (b) JS000-13, (c) JS142-23, and (d) JS153-38.

maximum difference between them is below 5.3%, confirming our experimental tests. It reveals that our numerical method can well capture the buckling and postbuckling features of damaged steel bars reinforced by

CFRP. This provides a robust numerical approach to explore other mechanical responses of steel-CFRP structures with imperfections under complicated environments that are inaccessible experimentally.

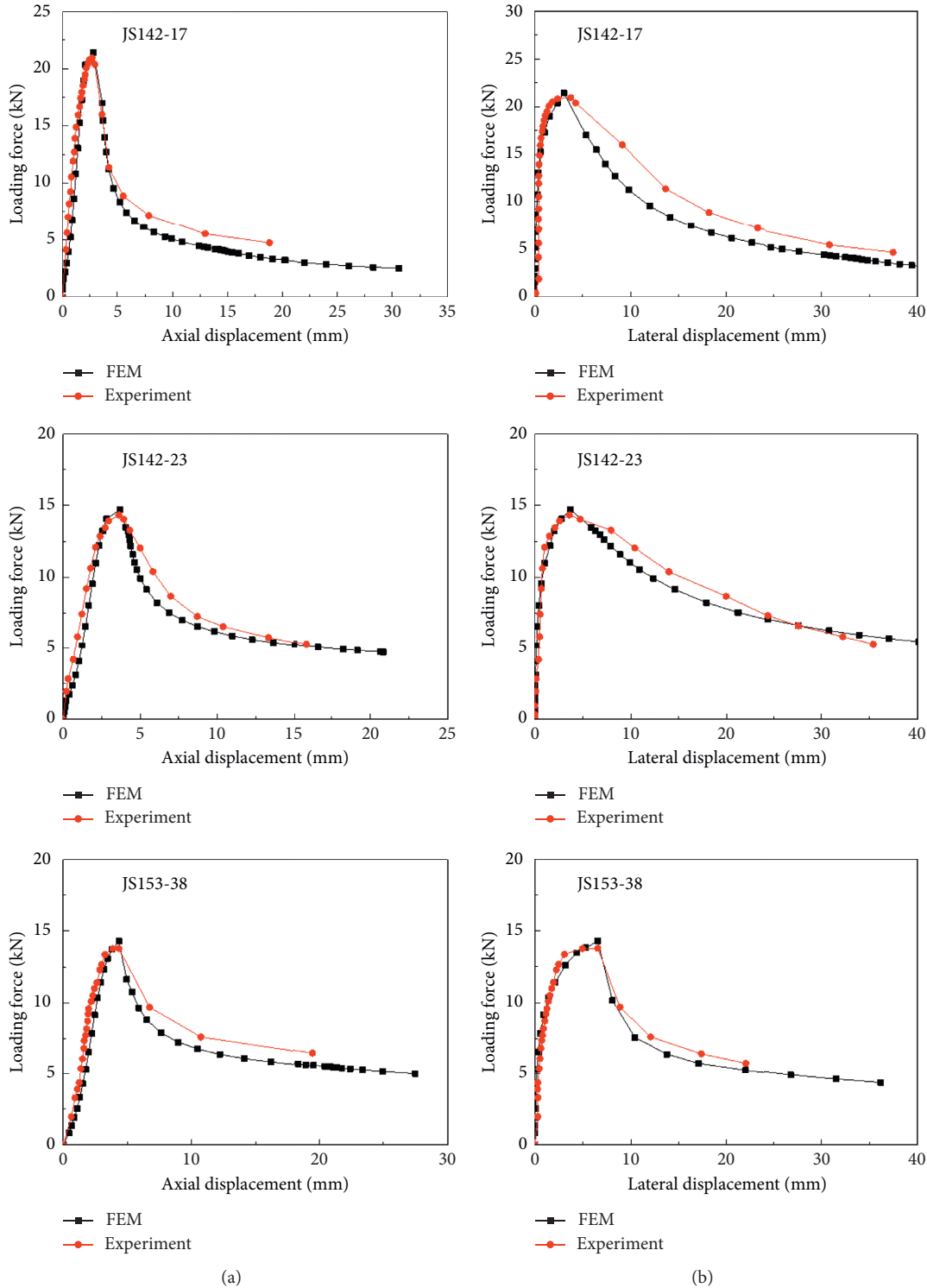


FIGURE 11: Comparison between finite element simulation and experimental results. (a) Axial displacement; (b) lateral displacement.

7. Conclusions

In the present study, we have examined the buckling and postbuckling behaviors of damaged steel bars reinforced with CFRP using experimental measurement, theoretical analysis, and numerical simulation. The critical force at

buckling onset and postbuckling characteristics are probed in three groups of 24 specimens subjected to axial compression. We demonstrate that the damage location and degree, CFRP layers, and reinforcement method play a significant role in the stability of steel bars. The theoretical prediction provides an upper bound for the critical force, in

consistency with our experimental measurement. We show that an optimized combination of these influence factors can remarkably enhance the stability of the damaged structures even beyond the undamaged counterparts. Our FEM simulations can not only predict the buckling mode and configuration but also quantitatively confirm the experimentally measured critical force and displacements. These findings provide important guides for designing steel-CFRP systems and strengthening damaged steel structures during later maintenance.

Finally, the bonding between steel and CFRP is perfectly retained during our experiment, theory, and simulation. It should be pointed out that CFRP delamination may happen in some other cases, which will weaken the reinforcement effect of CFRP. This issue merits further study in the future.

Data Availability

The experimental and simulation data used to support the findings of this study are included within the article and in the Supplementary Materials.

Conflicts of Interest

The authors declare that they have no known conflicts of financial interest or personal relationships that could have appeared to influence the work reported in this paper.

Acknowledgments

Bin Li acknowledges the supports from 973 Program of MOST (Grants nos. 2015CB057701 and 2015CB057702), University-Industry Collaborative Education Program of China (Grant no. (2020)6), Scientific Research Project of Hunan Provincial Department of Education (Grant no. (2020)), and Student Research Training Program of Hunan Province (Grant no. (2020)191).

Supplementary Materials

Figure S1: strains of the specimens in Group 2. Figure S2: strains of the specimens in Group 3. Table S1: influence of damage location on the critical force F_u . Table S2: influence of damage degree on the critical force F_u . Table S3: influence of CFRP players on the critical force F_u . Table S4: comparison between experiment (Exp) and FEM for specimens in Group 1. Table S5: comparison between experiment (Exp) and FEM for specimens in Group 2. Table S6: comparison between experiment (Exp) and FEM for specimens in Group 3. (*Supplementary Materials*)

References

- [1] D. Linghoff, R. Haghani, and M. Al-Emrani, "Carbon-fibre composites for strengthening steel structures," *Thin-Walled Structures*, vol. 47, no. 10, pp. 1048–1058, 2009.
- [2] A. Shaat and A. Z. Fam, "Slender steel columns strengthened using high-modulus CFRP plates for buckling control," *Journal of Composites for Construction*, vol. 13, no. 1, pp. 2–12, 2009.
- [3] J. G. Teng, T. Yu, and D. Fernando, "Strengthening of steel structures with fiber-reinforced polymer composites," *Journal of Constructional Steel Research*, vol. 78, pp. 131–143, 2012.
- [4] X.-L. Zhao and L. Zhang, "State-of-the-art review on FRP strengthened steel structures," *Engineering Structures*, vol. 29, no. 8, pp. 1808–1823, 2007.
- [5] X.-L. Zhao, D. Fernando, and R. Al-Mahaidi, "CFRP strengthened RHS subjected to transverse end bearing force," *Engineering Structures*, vol. 28, no. 11, pp. 1555–1565, 2006.
- [6] A. H. Al-Saidy, F. W. Klaiber, and T. J. Wipf, "Repair of steel composite beams with carbon fiber-reinforced polymer plates," *Journal of Composites for Construction*, vol. 8, no. 2, pp. 163–172, 2004.
- [7] S. El-Tawil, E. Ekiz, S. Goel, and S.-H. Chao, "Retraining local and global buckling behavior of steel plastic hinges using CFRP," *Journal of Constructional Steel Research*, vol. 67, no. 3, pp. 261–269, 2011.
- [8] Y. J. Kim and K. A. Harries, "Behavior of tee-section bracing members retrofitted with CFRP strips subjected to axial compression," *Composites Part B: Engineering*, vol. 42, no. 4, pp. 789–800, 2011.
- [9] C. Deng and W. Zhu, "Simplified buckling analysis of steel compression members strengthened with CFRP," *Industrial Construction*, vol. 38, pp. 106–108, 2008.
- [10] H. Ding, *Numerical Simulation Research on Stability Capacity of Hollow Section Columns Strengthened with CFRP*, Hefei University of Technology, Hefei, China, 2015.
- [11] K. A. Harries, A. J. Peck, and E. J. Abraham, "Enhancing stability of structural steel sections using FRP," *Thin-Walled Structures*, vol. 47, no. 10, pp. 1092–1101, 2009.
- [12] J. Hutchinson and W. Koiter, "Postbuckling theory," *Applied Mechanics Reviews*, vol. 23, pp. 1353–1366, 1970.
- [13] A. M. A. Van Der Heijden, *Koiter's Elastic Stability of Solids and Structures*, New York: Cambridge University Press, New York, NY, USA, 2009.
- [14] X. Q. Feng, Y. P. Cao, and B. Li, *Surface Wrinkling Mechanics of Soft Materials*, Science China Press, Beijing, China, 2017.
- [15] S. Kyriakides, C. D. Babcock, and D. Elyada, "Initiation of propagating buckles from local pipeline damages," *Journal of Energy Resources Technology*, vol. 106, no. 1, pp. 79–87, 1984.
- [16] W. Yuan, H. Song, L. Lu, and C. Huang, "Effect of local damages on the buckling behaviour of pyramidal truss core sandwich panels," *Composite Structures*, vol. 149, pp. 271–278, 2016.
- [17] S. Yu, Y. Ni, L. He, and Q.-L. Ye, "Tunable formation of ordered wrinkles in metal films with controlled thickness gradients deposited on soft elastic substrates," *ACS Applied Materials & Interfaces*, vol. 7, no. 9, pp. 5160–5167, 2015.
- [18] J. Wang, B. Li, Y. P. Cao, X. Q. Feng, and H. Gao, "Wrinkling micropatterns regulated by a hard skin layer with a periodic stiffness distribution on a soft material," *Applied Physics Letters*, vol. 108, Article ID 021903, 2016.
- [19] Y. Zhang, Z. Yan, K. Nan et al., "A mechanically driven form of Kirigami as a route to 3D meso structures in micro/nano membranes," *Proceedings of the National Academy of Sciences*, vol. 112, no. 38, pp. 11757–11764, 2015.
- [20] Y. Zhang, F. Zhang, Z. Yan et al., "Printing, folding and assembly methods for forming 3D mesostructures in advanced materials," *Nature Reviews Materials*, vol. 2, Article ID 17019, 2017.

- [21] F. Peng, J. Hao, Q. Yue, and Y. Yang, "Elastic stability analysis of axially loaded compression steel members by FRP strengthening," *Steel Construction*, vol. 20, pp. 18–21, 2005.
- [22] B. Li, C. X. Li, and C. L. Wei, "Stability analysis of steel compression members with local damage strengthened by FRP," *Steel Construction*, vol. 29, pp. 9–12, 2014.
- [23] S. P. Timoshenko and J. M. Gere, *Theory of Elastic Stability*, McGraw-Hill, New York, NY, USA, 1961.